EFFECTS OF LOCAL GEOLOGICAL CONDITIONS ON STRONG-GROUND MOTIONS IN THE VICINITY OF COALINGA, CALIFORNIA

R. D. Borcherdt, C. S. Mueller, and L. G. Wennerberg
U.S. Geological Survey
345 Middlefield Road, MS 77
Menlo Park, California

ABSTRACT

An array of six portable digital event recorders (GEOS) recorded eighteen aftershocks (M 1-4.3) during a three day deployment period to investigate the effects of local site conditions on earthquake-generated ground motions in the community of Coalinga. Large frequency-dependent amplitude variations due to local site conditions were observed over distances less than 1.5 km. The sites underlain by alluvium, including two sites in the community of Coalinga show evidence of site resonances with inferred amplifications of horizontal motion exceeding a factor of 10 in some cases. In general, the wide dynamic range broad-bandwidth signals recorded on the array show considerable amplification of the higher frequency components of shaking (5-15 Hz), suggesting that the alluvial deposits underlying the community of Coalinga could have been a contributory factor in the damage to old brick structures observed during the May 2, 1983 Coalinga earthquake.

INTRODUCTION

The moderate earthquake (M_L 6.5), which occurred on May 2, 1983 (23h 42m 37.85s GMT) approximately 10 km northeast of Coalinga, California, caused more than 30 million dollars in damage. A majority of the damage was associated with older unreinforced masonry structures located in Coalinga (Rojahn, oral commun.). As the community of Coalinga is underlain by a thick section of alluvium, a significant question for evaluation of earthquake-induced damage concerns the influence of local geological conditions. This paper provides a preliminary interpretation of ground motions generated by aftershocks of the

main event as recorded on wide-dynamic range, broad-bandwidth instrumentation (GEOS) located along a profile through the community of Coalinga.

GEOLOGIC SETTING AND STRONG MOTION DATA

The community of Coalinga is located in a northwest trending alluvial basin which serves as a surface expression of the Coalinga syncline. The basin is bounded on the northeast and southwest by sedimentary rocks of Tertiary and Cretaceous age which in turn are underlain by rocks of the Franciscan assemblage, which comprise the core of the Coalinga anticline. The damaging earthquake of May 2, 1983 occurred approximately 10 km northeast of Coalinga at a depth of 10.5 km (Eaton, 1983) beneath the surface axis of the Coalinga anticline.

To investigate the effects of the alluvial section underlying Coalinga on strong ground shaking, six recording stations were established along a profile extending from the heavily damaged area of Coalinga across the basin margin to a competent rock outcrop, approximately 4 km southwest of Coalinga (figure 1). The array was installed on May 19 and 20 and operated through May 23 as part of a larger strong-motion seismological study of the Coalinga aftershock sequence (Borcherdt and others, 1983).

Detailed information on alluvial thickness and seismic velocity structure had not been compiled as of this report; however, in general, the alluvial thickness is expected to be greatest at the northeastern end of the array (stations AAW, DZN) beneath the community of Coalinga and decrease toward the southwestern end (station LUC) (Rymer, oral commun.). Station TOT is located just beyond the margin of the alluvial basin on a thin veneer of soil underlain by sandstone (Rymer, oral commun.) Station FRS is located approximately 2 km from the alluvial margin of the basin in the hills on an outcrop of sandstone (Rymer, oral commun.).

Eighteen aftershocks were recorded by three or more stations during the three day deployment period. Twelve of these events were simultaneously recorded at station AAW located in Coalinga and at station FRS underlain by sandstone. Events of special interest are identified according to time of occurrence, 1222, 1005, and 0839, in figure 1 and table 1.

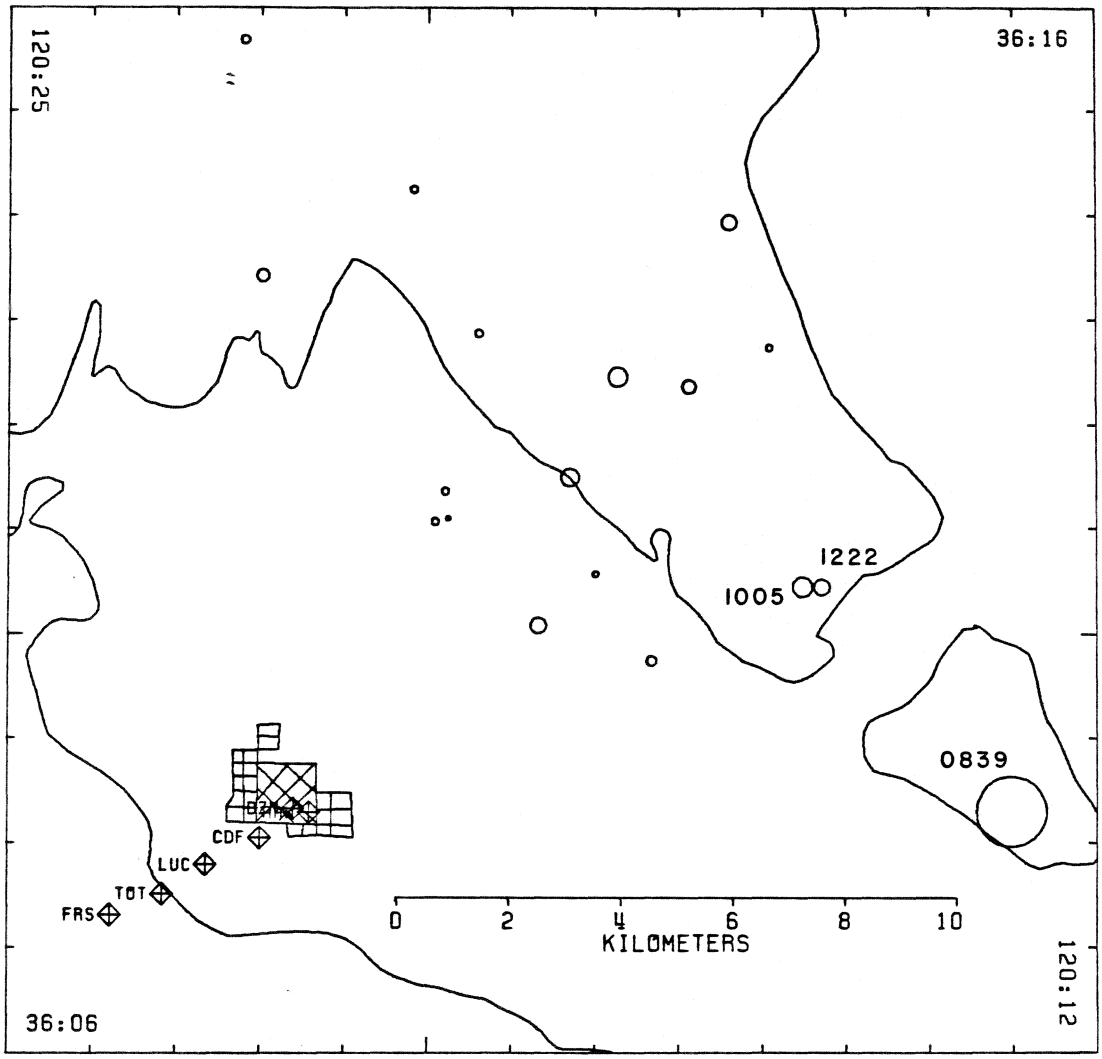

Figure 1. Location map for aftershocks recorded on a broad-band, digital array of six stations extending from the community of Coalinga to a nearby bedrock outcrop.

Table 1. Main event and some of the aftershocks recorded on the Coalinga array.

Event Time	M_L	Latitude Deg	Latitude Min	Longitude Deg	Longitude Min	Depth km	Dist AAW km
122 2342	6.5	36	13.99	120	17.59	10.5	12.1
140 1222	3.0	36	10.45	120	15.29	9.2	13.6
141 1005	3.2	36	10.45	120	15.52	9.7	13.7
141 2000	3.0	36	10.08	120	18.67	7.2	9.0
142 0839	4.3	36	08.30	120	13.02	9.3	15.7
142 0950	2.3	36	11.06	120	19.91	5.6	7.9
143 1327	3.1	36	11.49	120	18.30	8.3	11.2

The array of instrumentation was comprised of six portable digital recorders (GEOS) (Borcherdt and others, 1979). Each system was equipped to record three components of ground motion as detected by two sets of sensors (velocity transducers and force-balanced accelerometers). Utilization of two sets of sensors permits the microcomputer based recording system to record on-scale seismic signals ranging from that of the seismic background noise to the upper limit of the accelerometers (> 1g) with 16 BIT (96 db) signal resolution without change in gain settings. The wide dynamic range and broad frequency bandwidth of the recorded signals provides a unique opportunity to investigate the high-frequency response of an alluvial basin.

ANALOG AMPLIFICATIONS

Three components of ground velocity generated by the largest aftershock recorded on the array (142 0839, M_L 4.3) are shown for five of the array stations (figures 2a, 2b, and 2c). Visual comparison of the time histories shows that, in general, the amplitudes and durations of the velocity time histories are greater for the sites underlain by alluvium (AAW, DZN, LUC) than those for sandstone (FRS). The apparent soil amplification effects are greater for the horizontal components of motion than for the vertical components. Station TOT near the margin of the basin shows vertical amplitudes greater than those on the alluvial sites, but horizontal amplitudes comparable or less than those at the alluvial sites. It should be pointed out that the horizontal velocity recordings for stations LUC and TOT are "clipped" due to gain settings inappropriate for the dyamic range and sensitivity of the velocity transducers. Calculation of soil responses for this event will be based on recordings of the force-balanced accelerometers to be discussed in a later section.

A similar set of recordings for a smaller event (141 1005 M_L 3.2) located more inline with the array profile (figure 1) is shown in figures 3a, 3b, and 3c. Similarly, these time histories suggest that the ground velocities recorded on the alluvial sites are several times larger than those observed on the sandstone site with the largest time-history amplitudes occurring for the horizontal components of ground velocity recorded at the sites AAW and DZN located in Coalinga. The maximum peak-to-peak amplitudes observed for events of magnitude greater than 2.5 are tabluated (table 2). Corresponding ratios

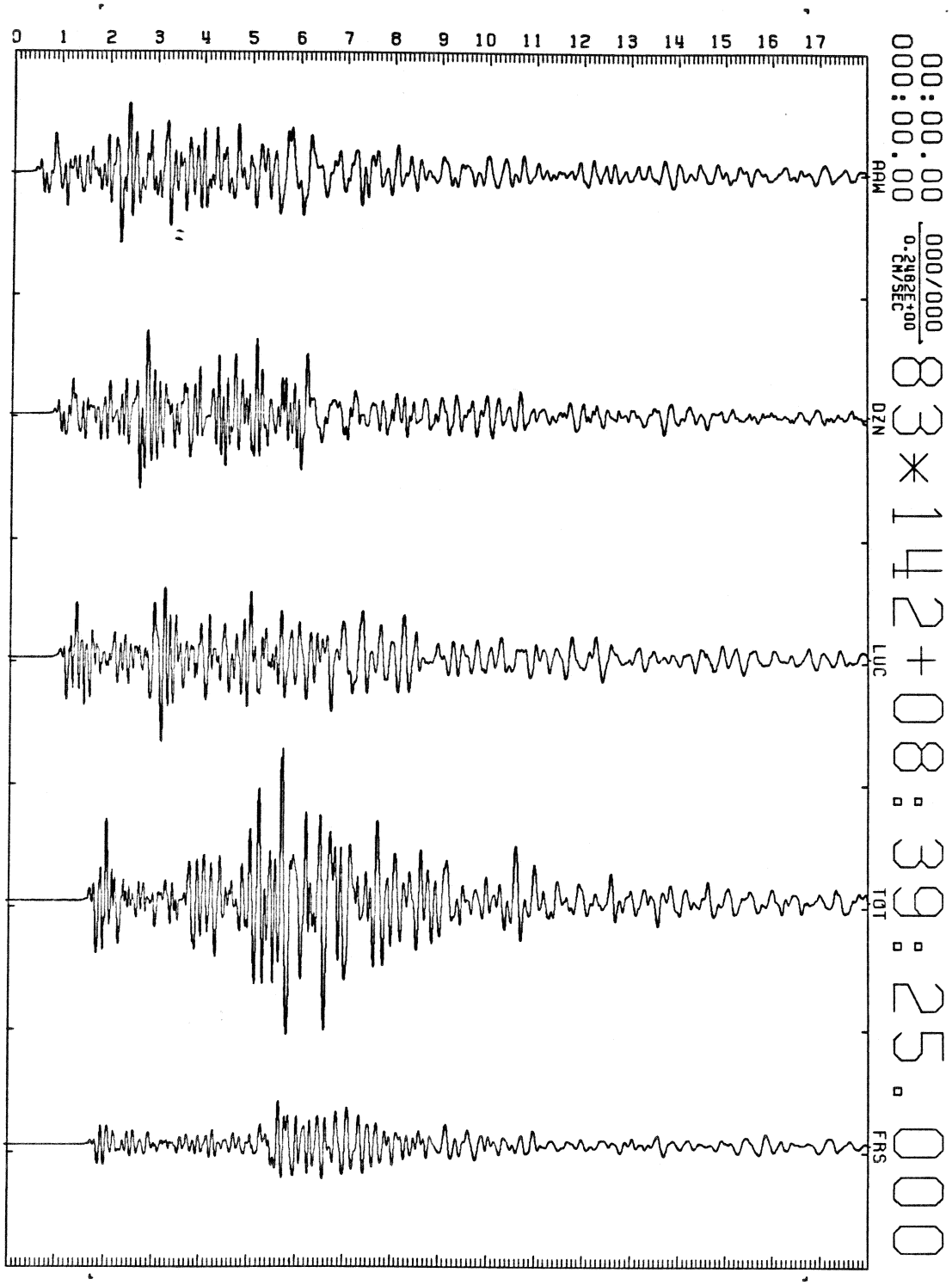

Figure 2a. Three components of ground velocity generated by a magnitude 4.3 event (0839, figure 1) as recorded on five wide-dynamic range broad-bandwidth digital instruments (GEOS). Equiscaled recordings of the vertical (figure 2a), east-west (figure 2b), and north-south (figure 2c) components of ground motion are shown.

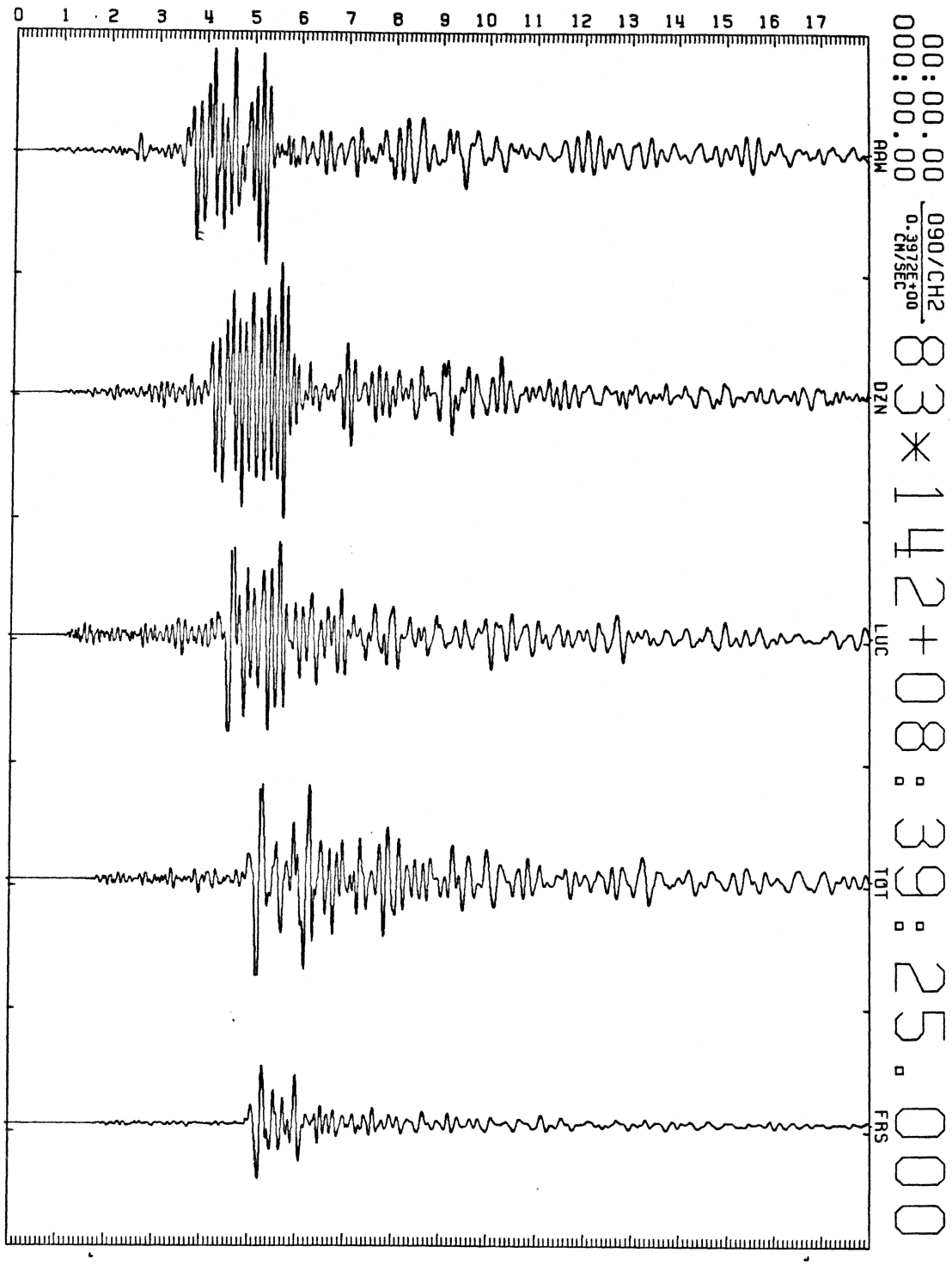

Figure 2b. Three components of ground velocity generated by a magnitude 4.3 event (0839, figure 1) as recorded on five wide-dynamic range broad-bandwidth digital instruments (GEOS). Equiscaled recordings of the vertical (figure 2a), east-west (figure 2b), and north-south (figure 2c) components of ground motion are shown.

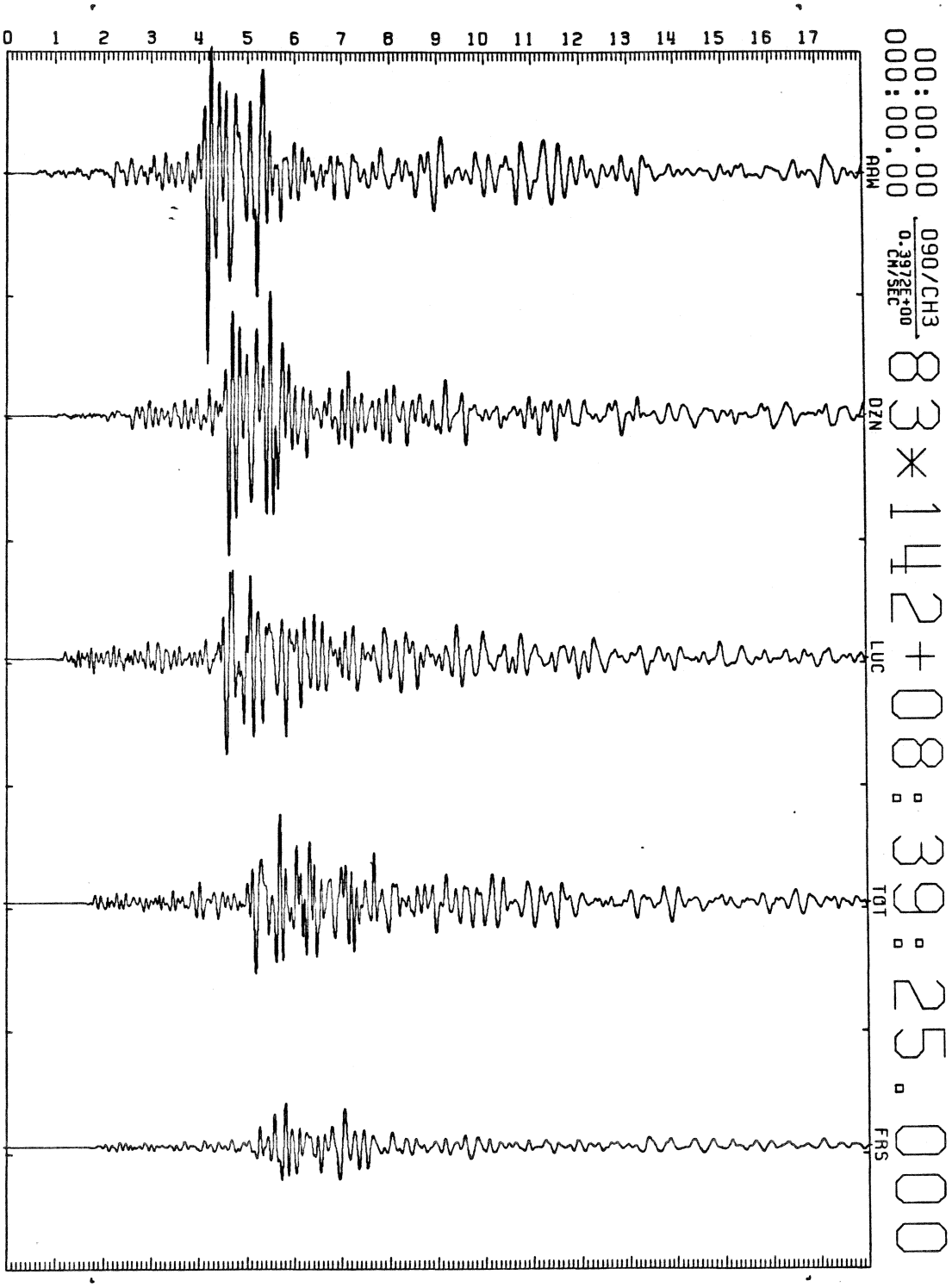

Figure 2c. Three components of ground velocity generated by a magnitude 4.3 event (0839, figure 1) as recorded on five wide-dynamic range broad-bandwidth digital instruments (GEOS). Equiscaled recordings of the vertical (figure 2a), east-west (figure 2b), and north-south (figure 2c) components of ground motion are shown.

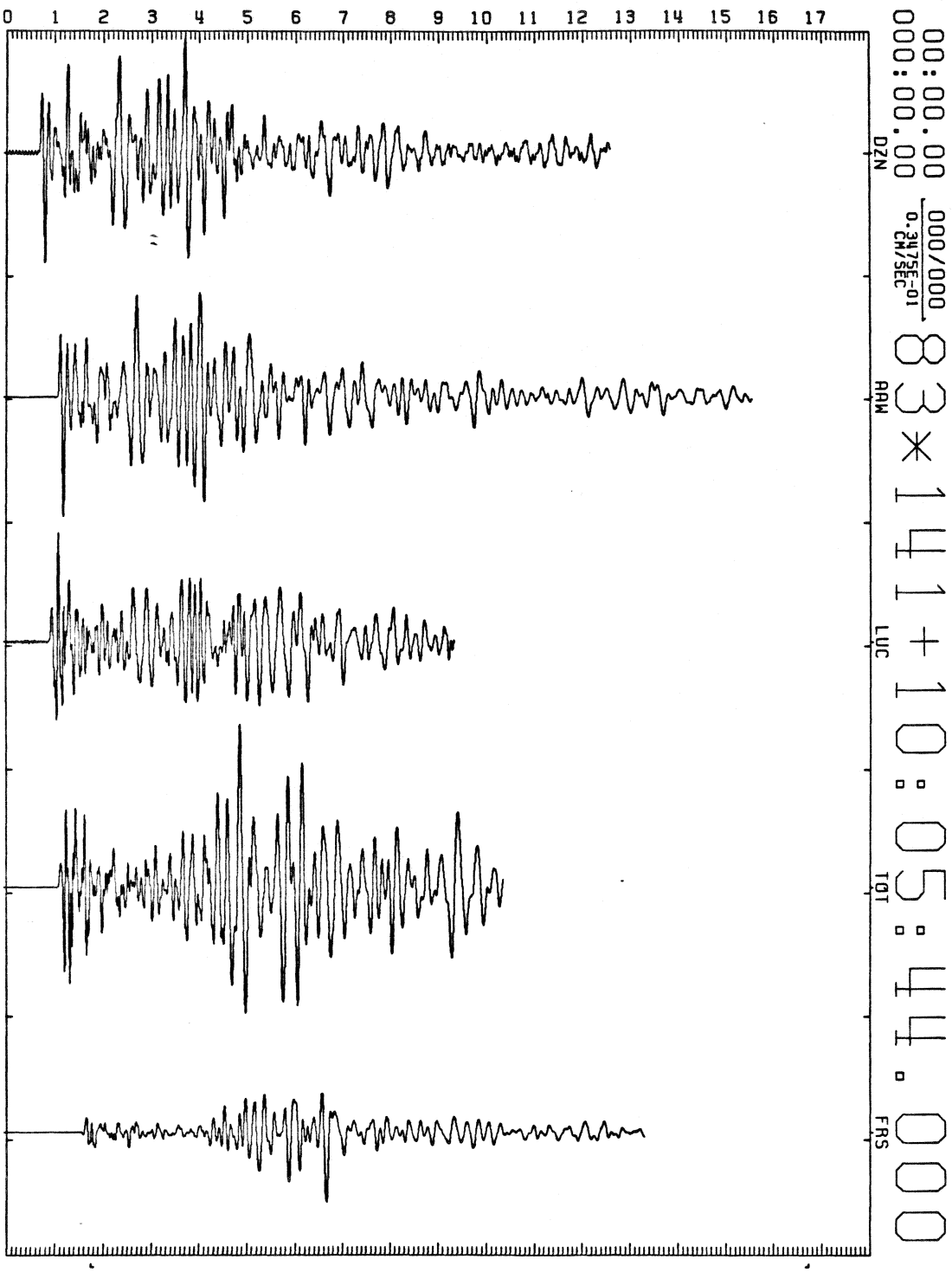

Figure 3a. Three components of ground velocity generated by a magnitude 3.2 event (1005, figure 1) as recorded on five wide-dynamic range broad-bandwidth digital instruments (GEOS). Equiscaled recordings of vertical (figure 3a), east-west (figure 3b), and north-south (figure 3c) components of ground motion are shown.

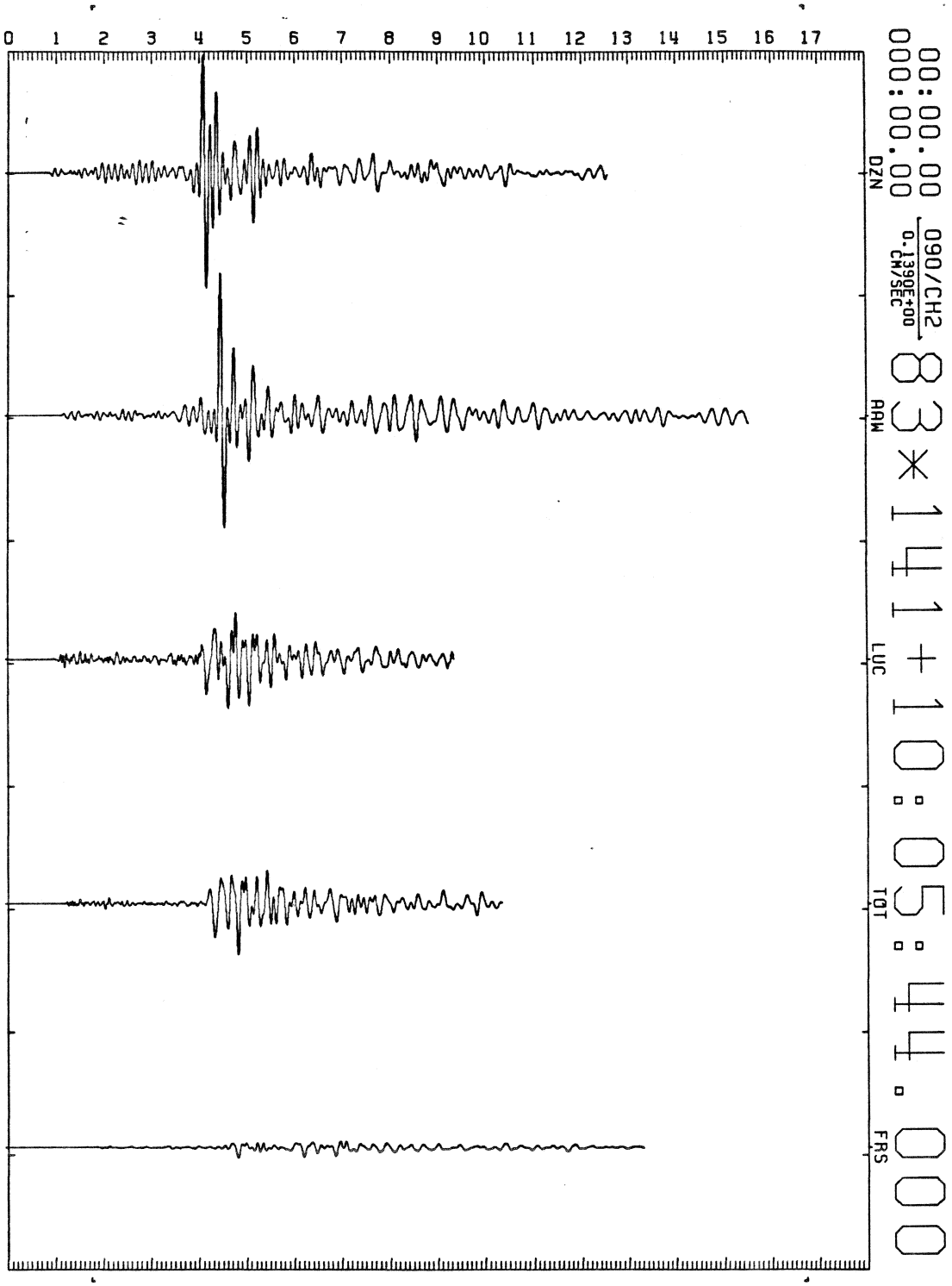

Figure 3b. Three components of ground velocity generated by a magnitude 3.2 event (1005, figure 1) as recorded on five wide-dynamic range broad-bandwidth digital instruments (GEOS). Equiscaled recordings of vertical (figure 3a), east-west (figure 3b), and north-south (figure 3c) components of ground motion are shown.

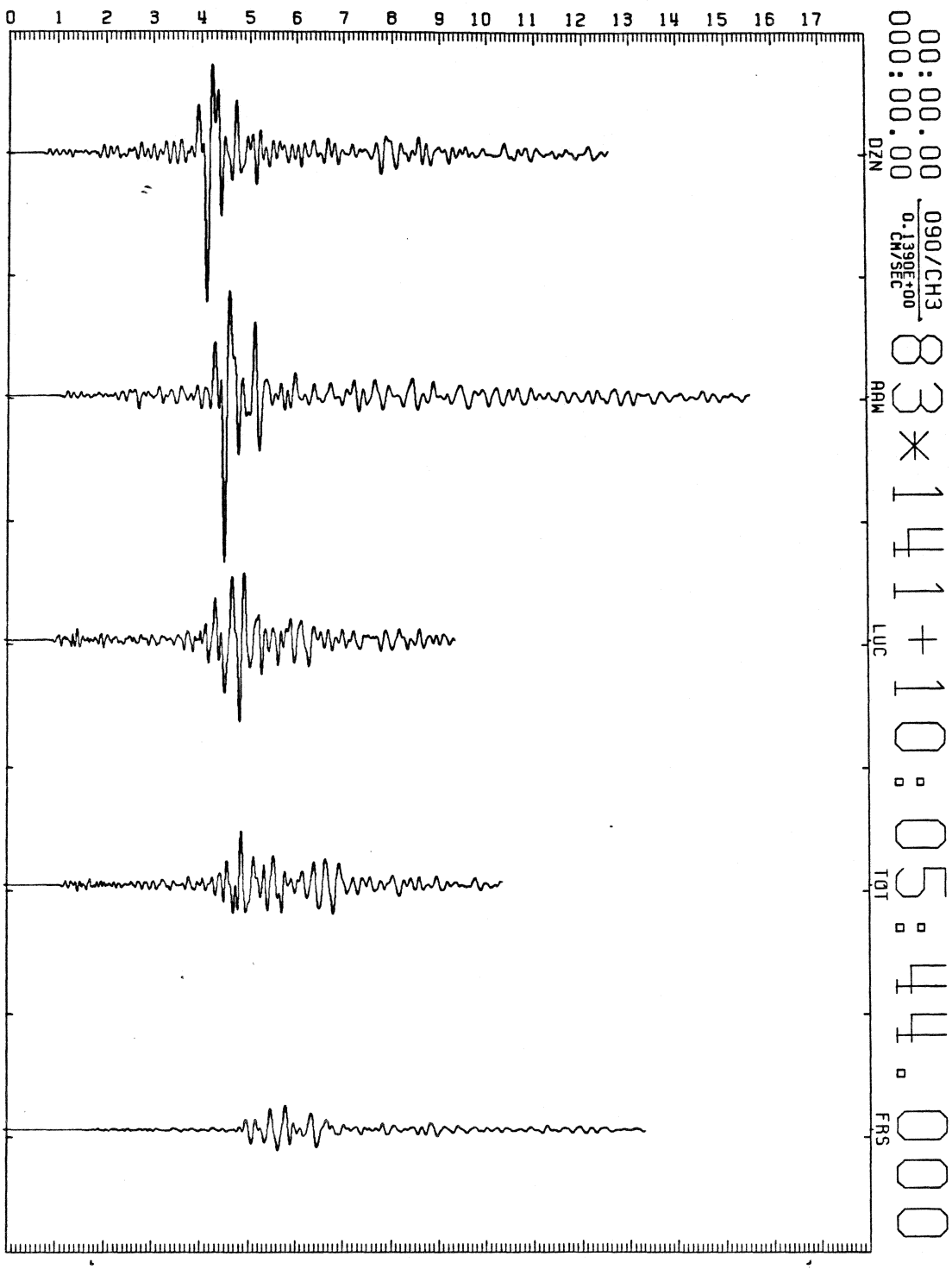

Figure 3c. Three components of ground velocity generated by a magnitude 3.2 event (1005, figure 1) as recorded on five wide-dynamic range broad-bandwidth digital instruments (GEOS). Equiscaled recordings of vertical (figure 3a), east-west (figure 3b), and north-south (figure 3c) components of ground motion are shown.

with respect to station FRS and scaled to account for geometrical spreading are also tabulated (table 2, cols. 3-6). Events 140 1222 and 141 1005 are of similar magnitude, depth, and azimuth with respect to the array (see table 1 and figure 1). Event 142 0839 is of larger magnitude (M_L 4.3 vs 3), comparable depth, comparable distance, and along a more easterly azimuth more in line with the long axis of the alluvial basin. In the case of the magnitude 4.3 event (142 0839) the variations in normalized amplitudes from those for events 140 1222 and 141 1005 suggest that source location with respect to syncline axis may be a significant factor in relative ground response observed on the array.

Averages computed at each site for the nine events with $M_L \geq 2.5$ (table 2) suggest the amplifications of vertical motion increase with decreasing thickness of alluvium with the largest amplifications occurring at the margin of the basin. Inversely, the horizontal amplifications increase with increasing thickness and are largest for the sites in Coalinga.

Examples of the Fourier amplitude spectra scaled to the hypocentral distance of station FRS are shown for three components of acceleration generated by the magnitude 4.3 event for station AAW (downtown Coalinga) (figure 4a) and station FRS (figure 4b). Inspection of the amplitude spectra computed for all of the recorded time histories suggests that a seismic signal level significantly above the seismic noise level can be expected in the frequency bandwidth of 0.5-25 Hz.

Instrumentation response curves computed from calibration signals automatically recorded at each of the stations provide an accurate means of estimating variations in observed amplitude due to variations in instrumentation response at the time events are recorded. Examples of the instrumentation response to a step function in acceleration applied to the velocity transducers for stations AAW and FRS are illustrated in figures 5a and 5b. Comparison of the curves shows that the amplitude response for the systems are similar, but subtle variations suggest that instrument calibration at the time of data recovery is useful for comparative ground motion measurements. Previous comparative studies by Borcherdt (1970) using analog instrumentation have shown a similar result.

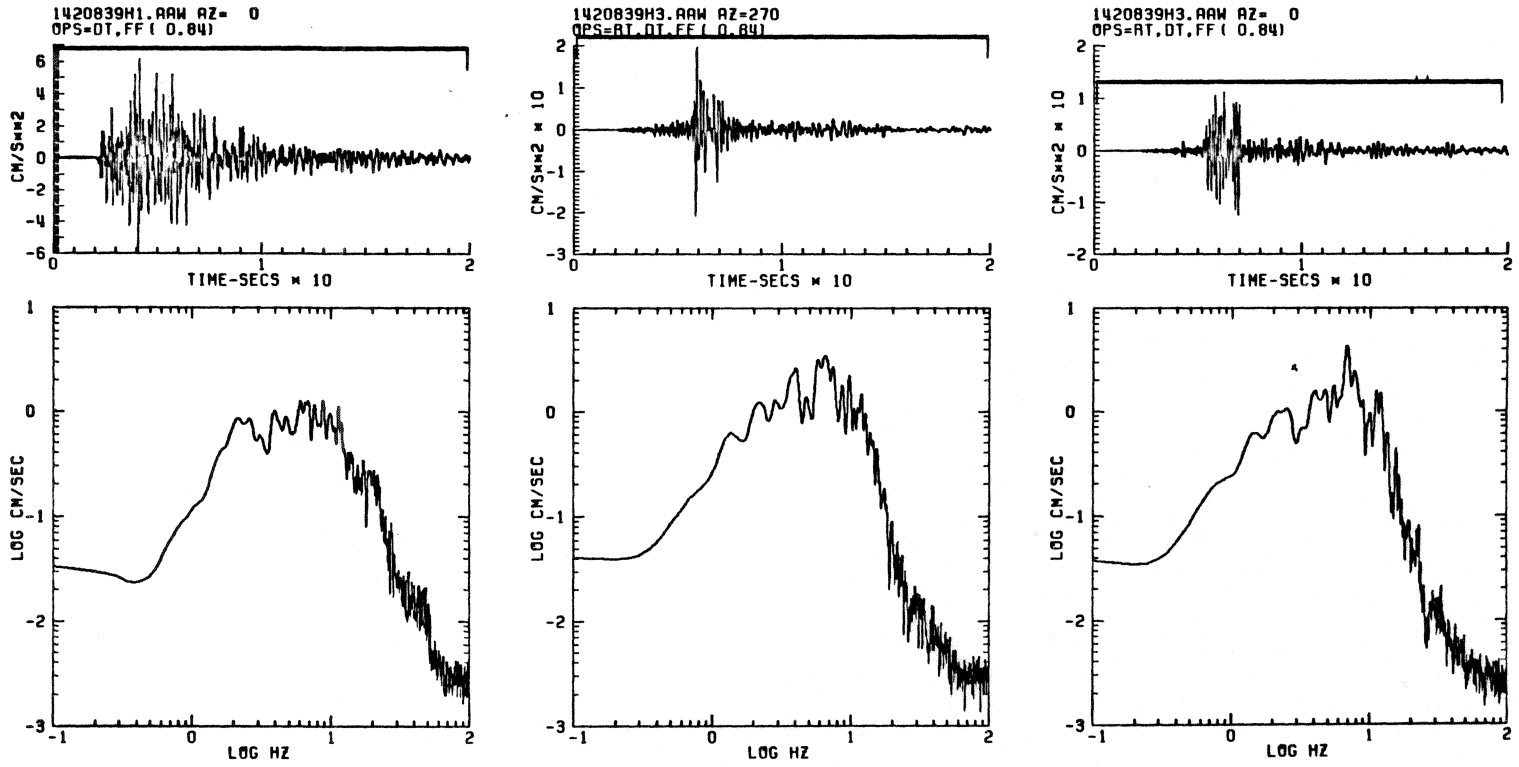

Figure 4a. Fourier amplitude and acceleration time histories for the three components of ground acceleration recorded at site AAW in Coalinga (figure 4a) and at the rock site FRS (figure 4b).

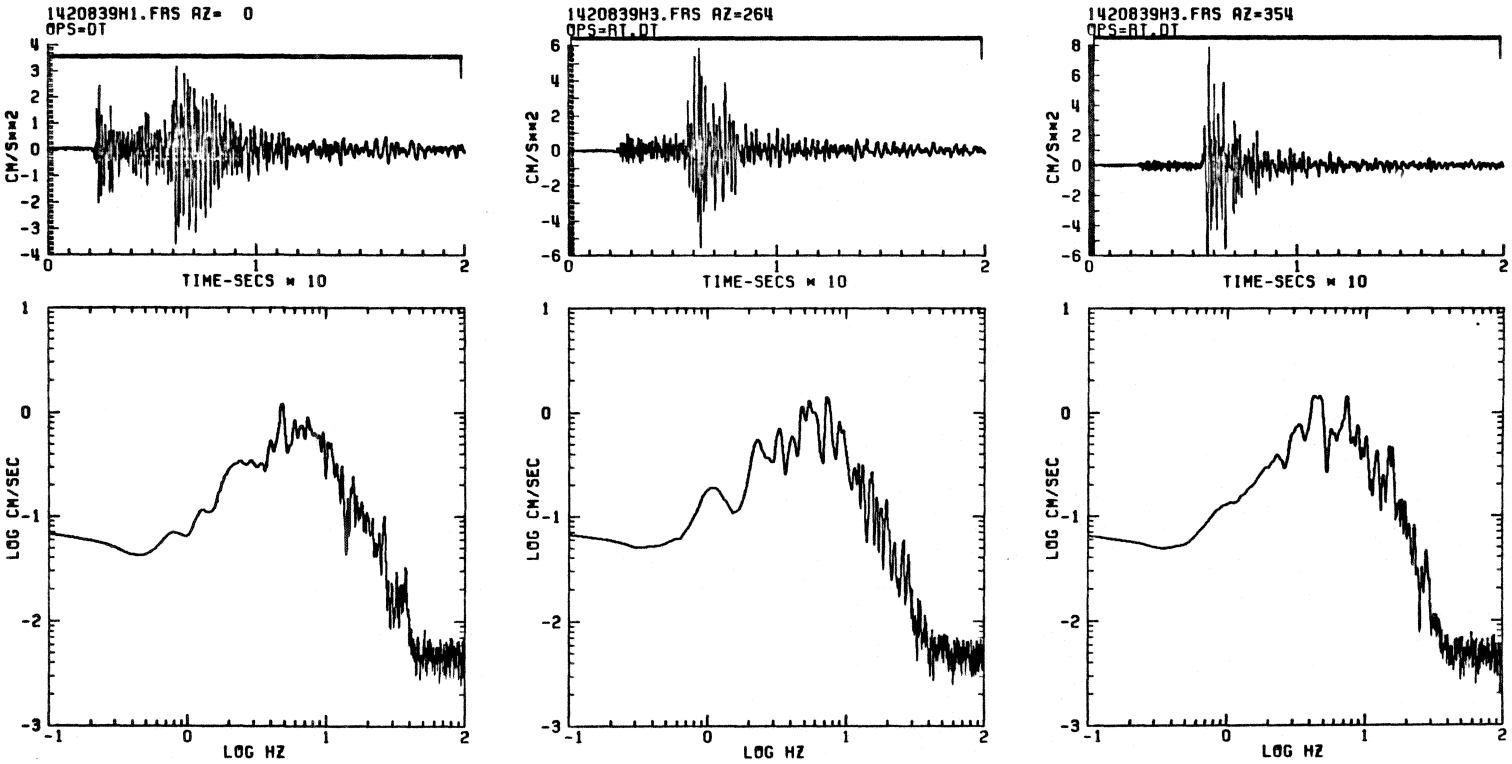

Figure 4b. Fourier amplitude and acceleration time histories for the three components of ground acceleration recorded at site AAW in Coalinga (figure 4a) and at the rock site FRS (figure 4b).

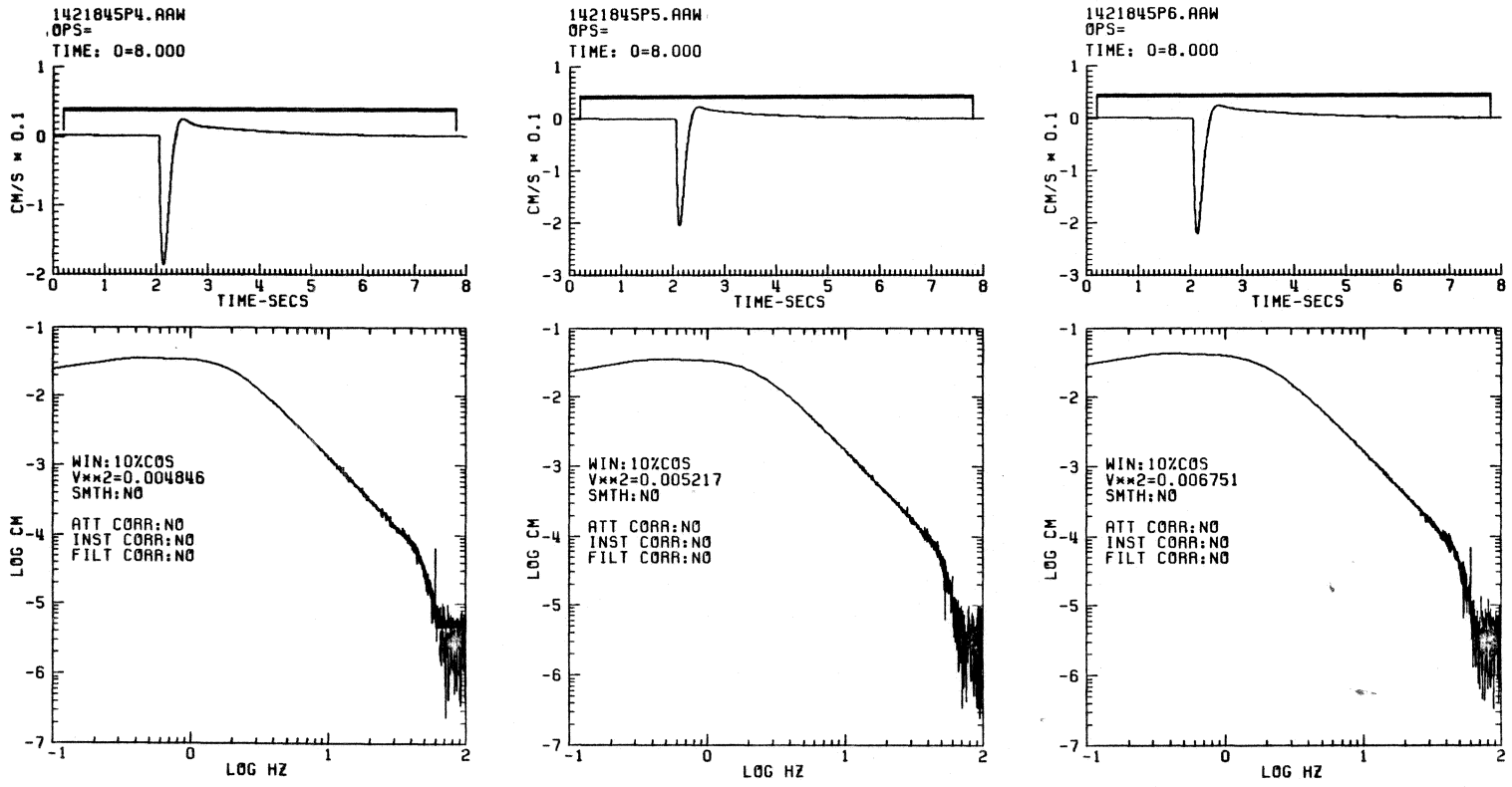

Figure 5a. Time history and Fourier amplitude response of GEOS recording system to step function in acceleration applied to velocity transducer automatically in the field at stations AAW (figure 5a) and FRS (figure 5b).

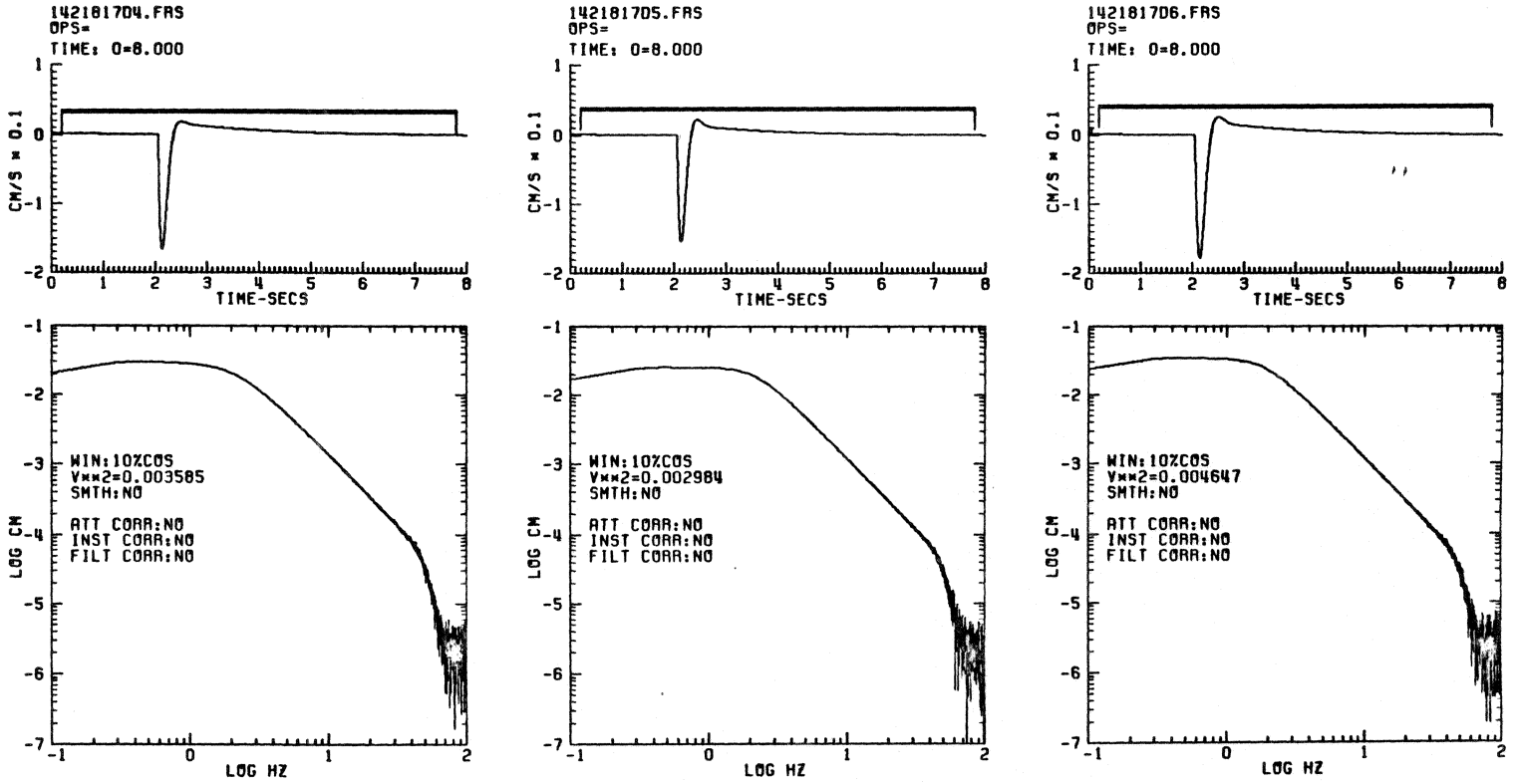

Figure 5b. Time history and Fourier amplitude response of GEOS recording system to step function in acceleration applied to velocity transducer automatically in the field at stations AAW (figure 5a) and FRS (figure 5b).

SPECTRAL AMPLIFICATIONS

To better isolate the effects of local site conditions from those of sensor, recording instrument, seismic source, and propagation path, Fourier amplitude spectral ratios were computed with respect to station FRS underlain by sandstone. To account for variations in amplitude due to geometrical spreading the amplitude spectra were scaled to correspond to the hypocentral distance of station FRS. Examples of the vertical component spectral ratios are shown for two magnitude 3 events (140 1222 and 141 1005) and the magnitude 4.3 event (142 0839) (in figure 6). The radial and transverse component spectral ratios for these events are shown in figures 7 and 8.

The spectral ratios for the two magnitude 3 events (140 1222 and 141 1005) which occurred in about the same location (see figure 1) are very nearly the same for each of the sites, especially for frequencies less than 15 Hz (compare figures 6a and 6b, 7a and 7b, and 8a and 8b). However, the spectral ratios for the magnitude 4.3 event (142 0839) when compared to those for the magnitude 3 events show significant variations as a function of frequency with evidence for possible reasonances, especially for frequencies greater than 5 Hz (compare figures 6b and 6c, 7b and 7c, and 8b and 8c). The variations in the spectral ratios shown for the three events suggests that the high-frequency response (> 5 Hz) of the soil sites is strongly dependent on both source location and near-surface velocity structure pertinent to various propagation paths. A more detailed interpretation of the spectral ratios must await compilation of information on near-surface velocity structure, basin geometry, and estimates of source radiation characteristics.

To summarize the amplifications observed for a larger sample of events than those for which spectral ratios were computed, means and standard deviations are plotted for the analog ratios of peak ground motions (table 2) determined relative to station FRS for all events of magnitude greater than 2.5 (figures 9a, 9b, and 9c). The mean amplification ratios suggest that in general the mean horizontal soil site decrease from about a factor of 5 for the sites in Coalinga to about a factor of 3 for the site TOT on the margin of the basin. Mean analog amplifications of the vertical motion show an inverse relation with the largest amplifications occurring for site TOT.

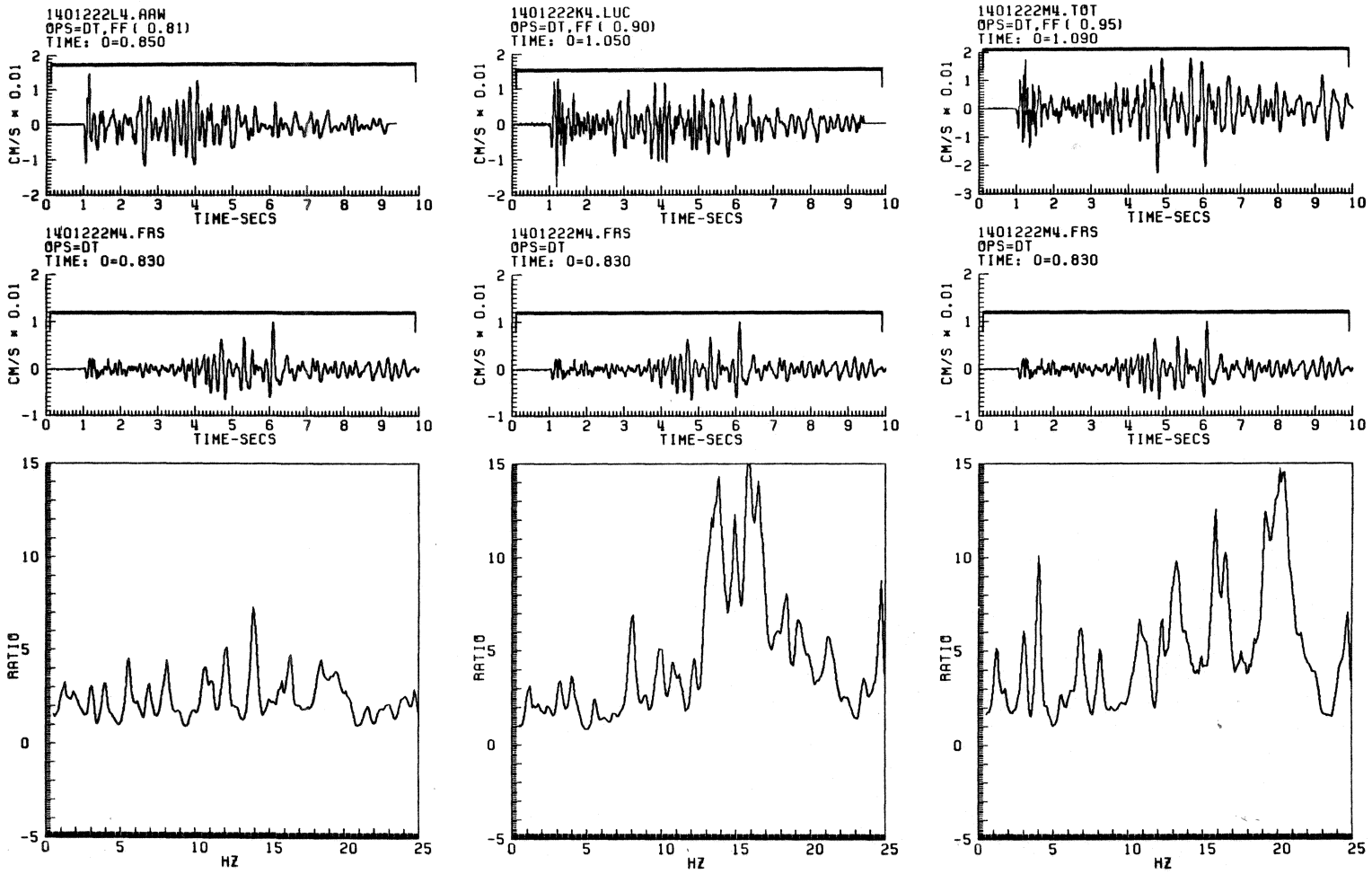

Figure 6a. Time histories and amplitude spectral ratios computed for vertical component of motion at sites AAW, LUC, and TOT generated by event 1222 (figure 6a), event 1005 (figure 6b) and event 0839 (figure 6c).

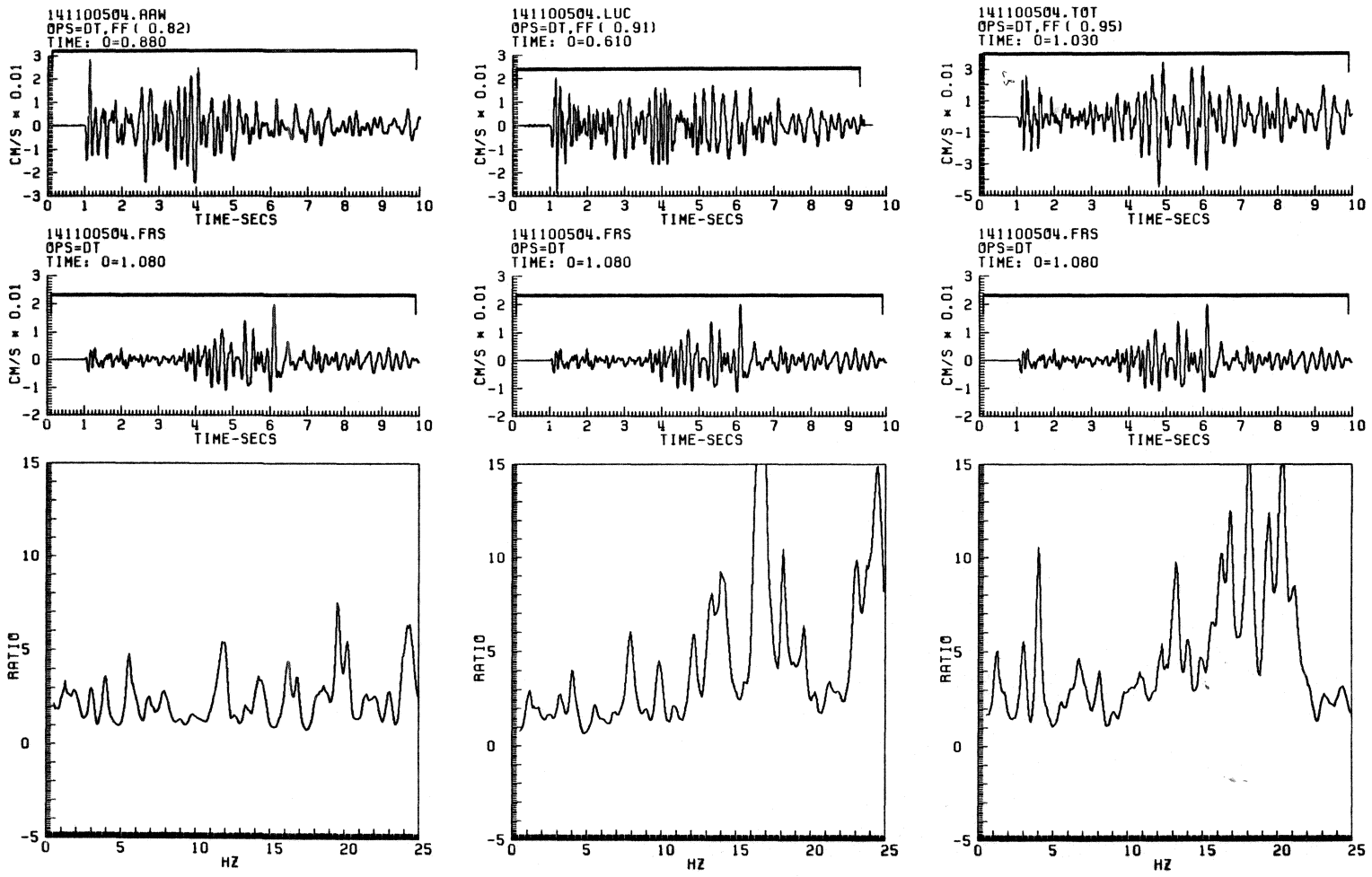

Figure 6b. Time histories and amplitude spectral ratios computed for vertical component of motion at sites AAW, LUC, and TOT generated by event 1222 (figure 6a), event 1005 (figure 6b) and event 0839 (figure 6c).

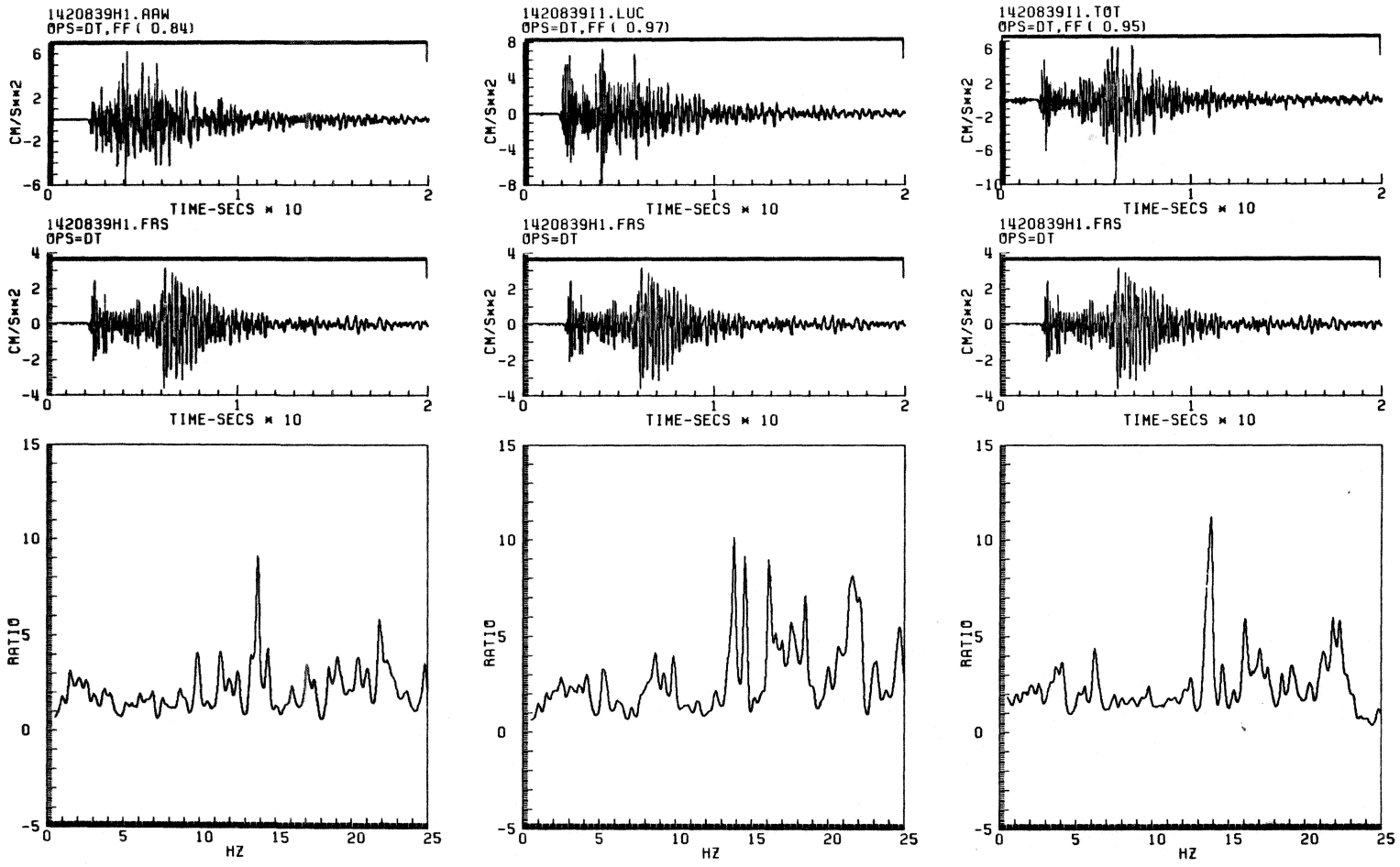

Figure 6c. Time histories and amplitude spectral ratios computed for vertical component of motion at sites AAW, LUC, and TOT generated by event 1222 (figure 6a), event 1005 (figure 6b) and event 0839 (figure 6c).

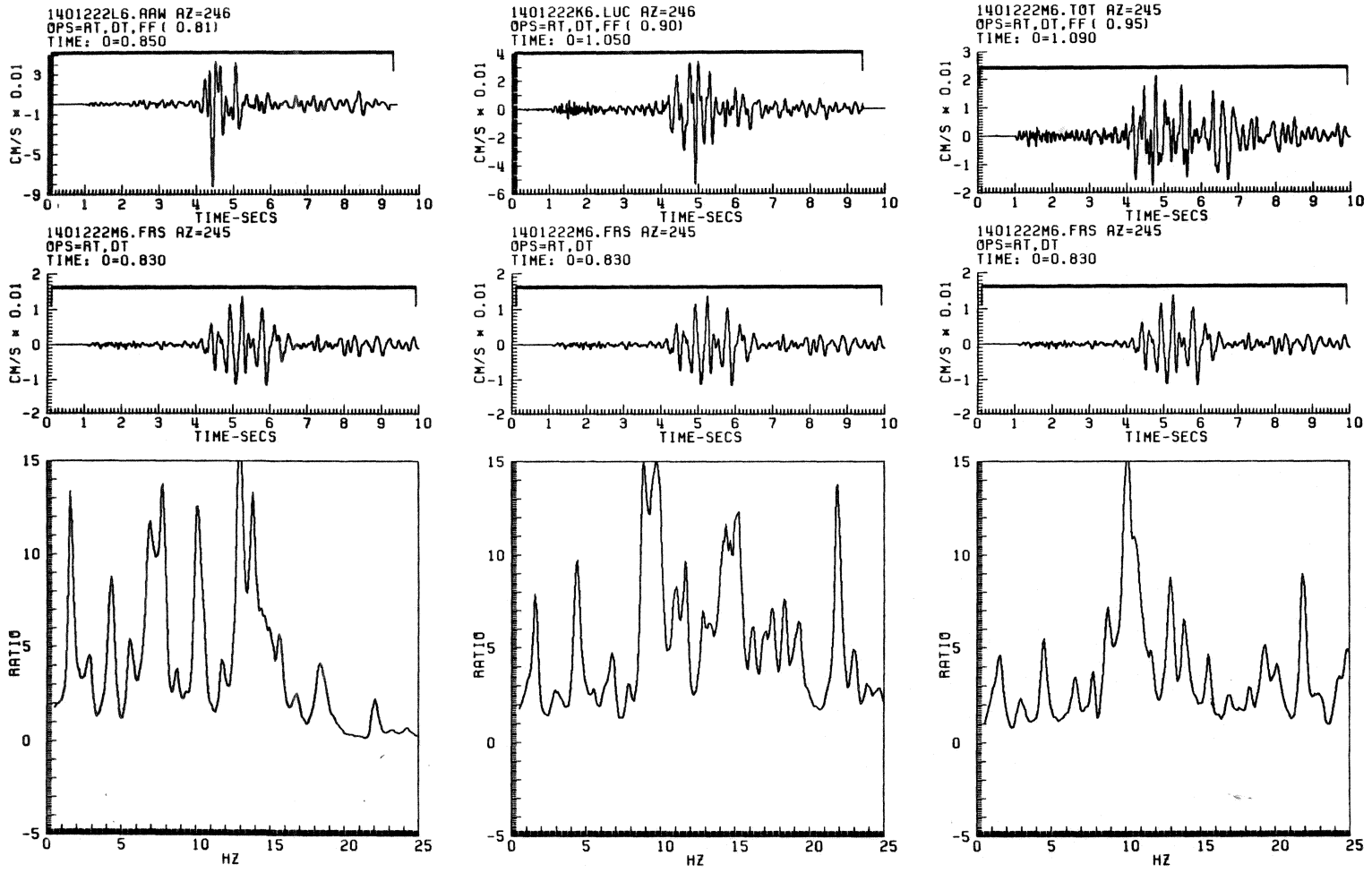

Figure 7a. Time histories and amplitude spectral ratios computed for radial component of motion at sites AAW, LUC, and TOT generated by event 1222 (figure 7a), event 1005 (figure 7b) and event 0839 (figure 7c).

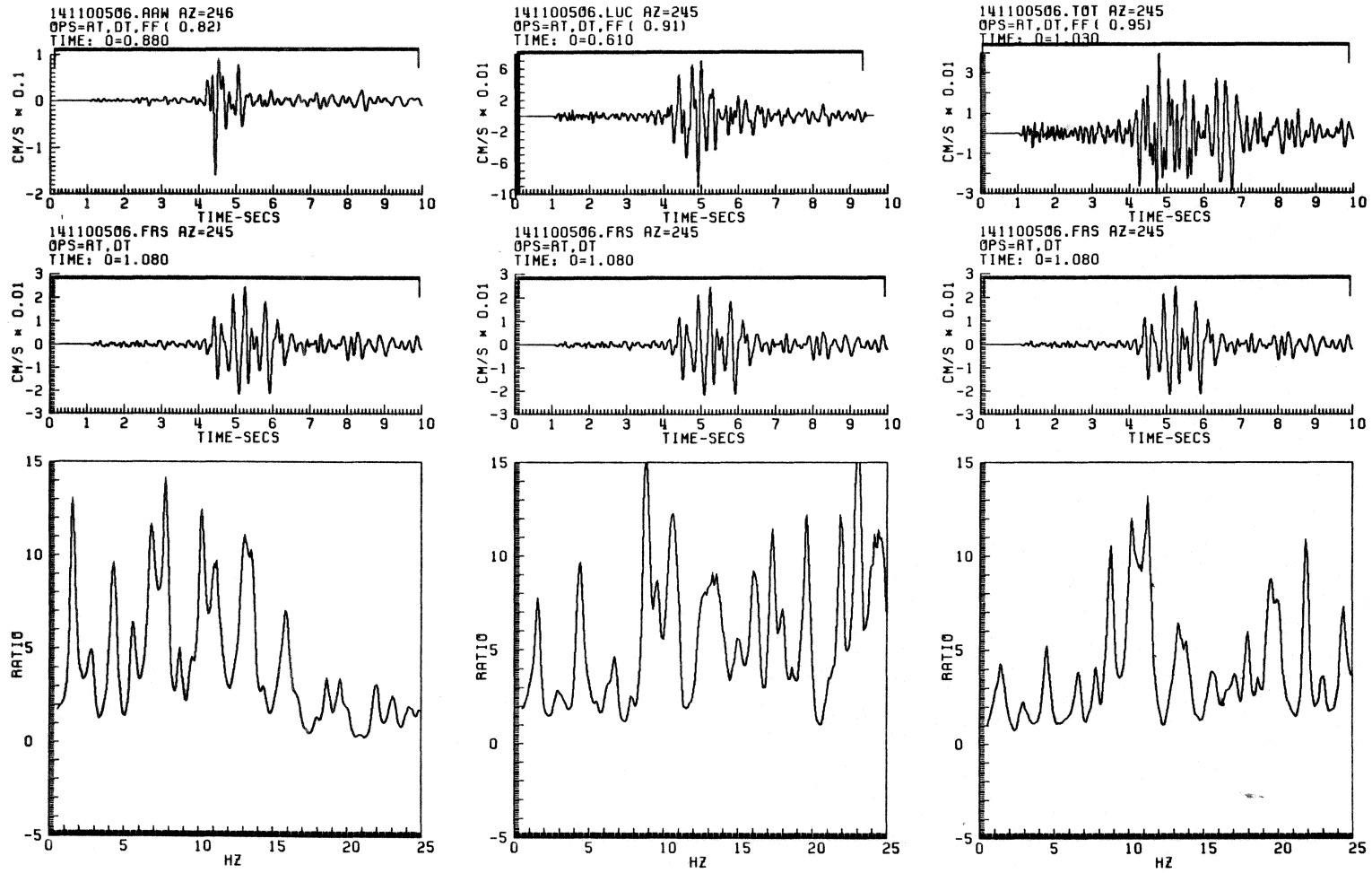

Figure 7b. Time histories and amplitude spectral ratios computed for radial component of motion at sites AAW, LUC, and TOT generated by event 1222 (figure 7a), event 1005 (figure 7b) and event 0839 (figure 7c).

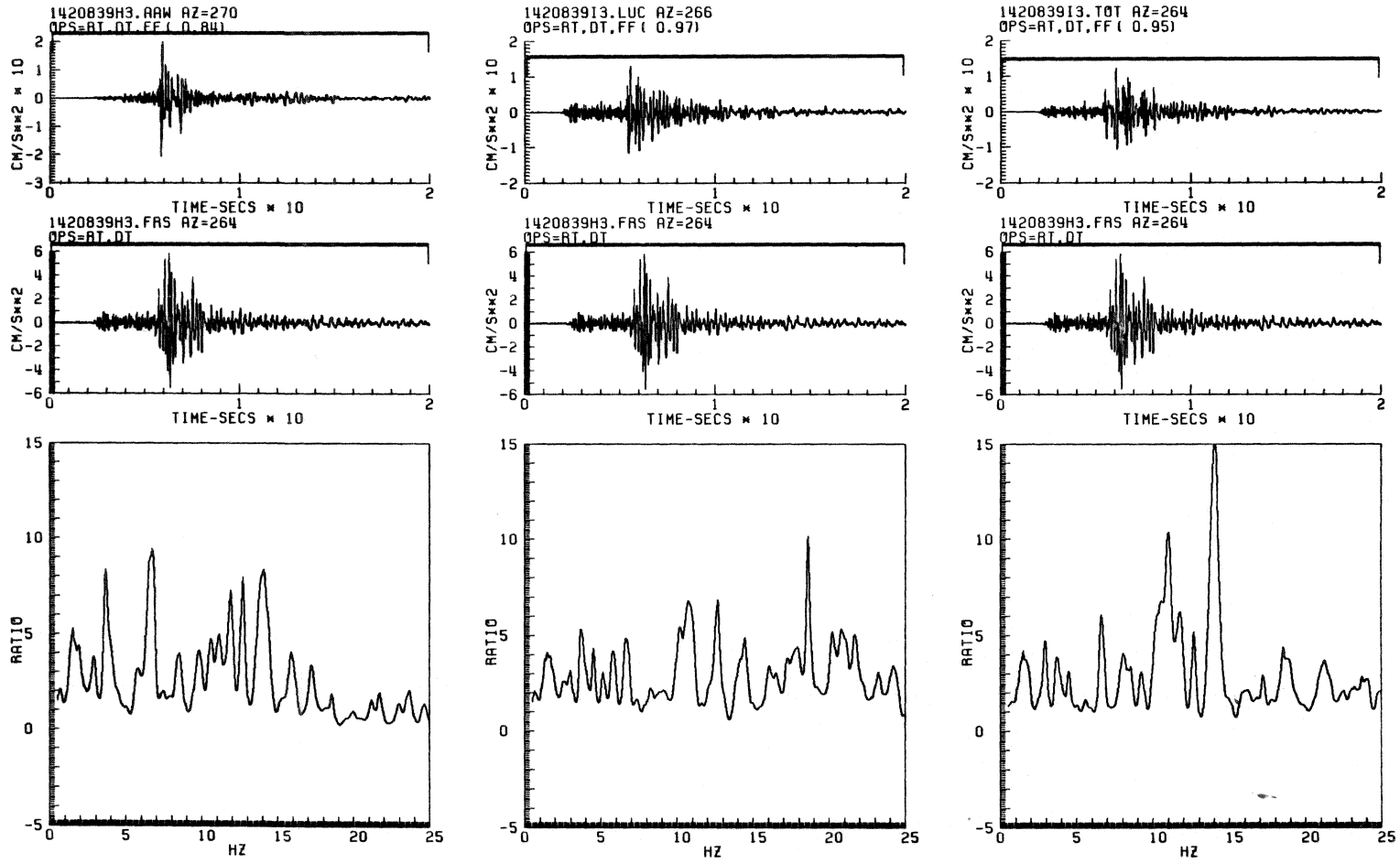

Figure 7c. Time histories and amplitude spectral ratios computed for radial component of motion at sites AAW, LUC, and TOT generated by event 1222 (figure 7a), event 1005 (figure 7b) and event 0839 (figure 7c).

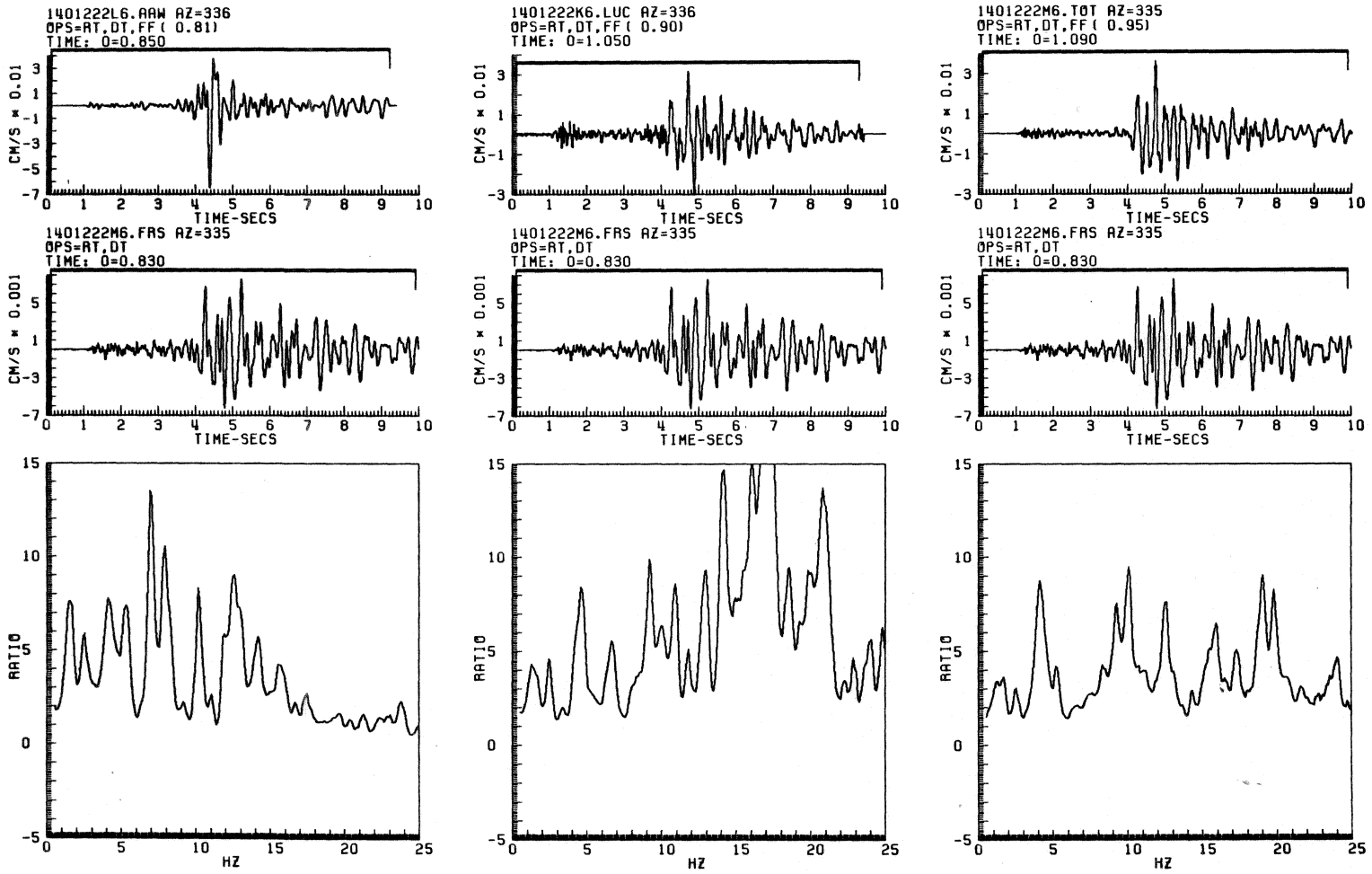

Figure 8a. Time histories and amplitude spectral ratios computed for transverse component of motion at sites AAW, LUC, and TOT generated by event 1222 (figure 8a), event 1005 (figure 8b) and event 0839 (figure 8c).

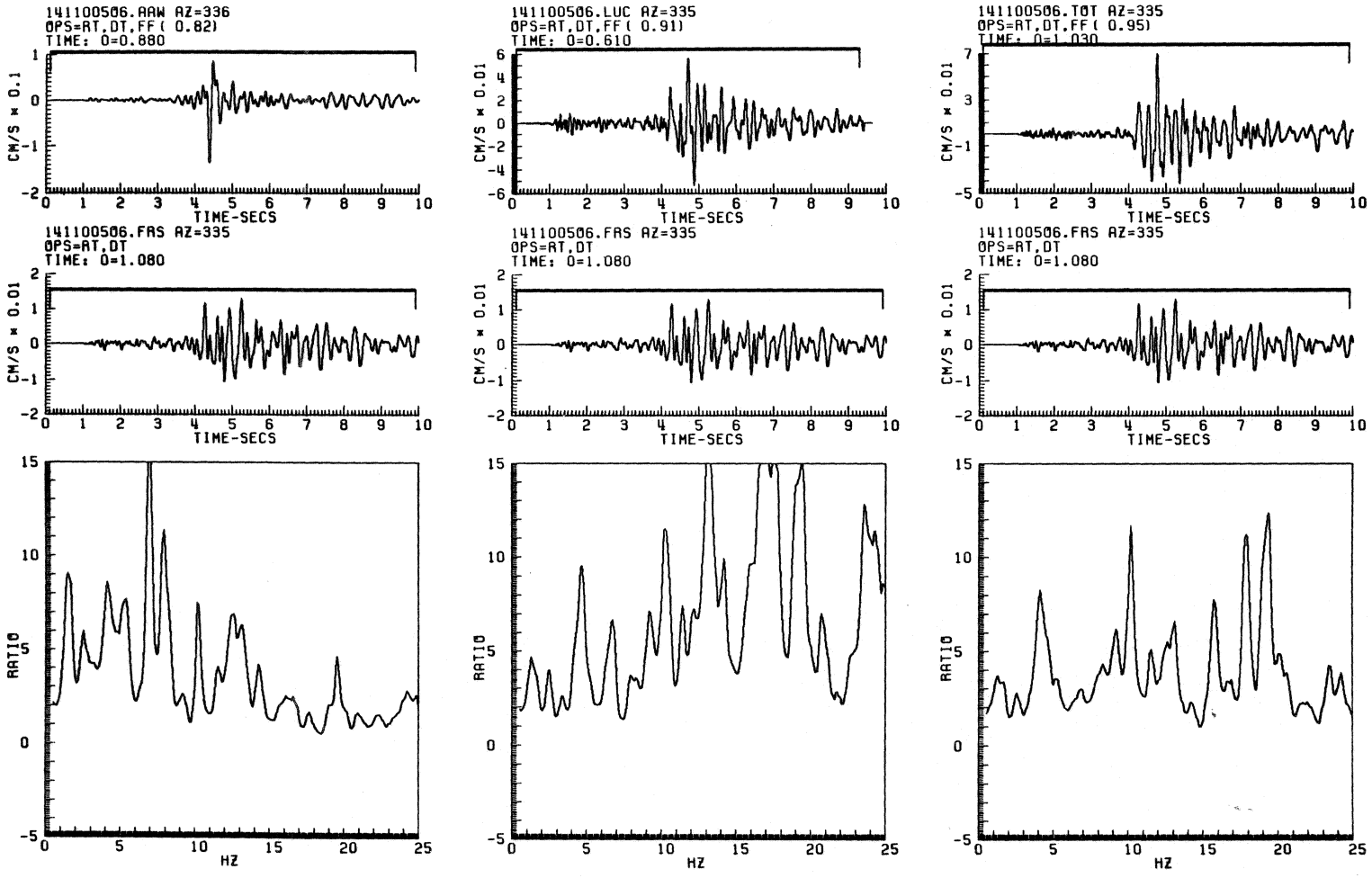

Figure 8b. Time histories and amplitude spectral ratios computed for transverse component of motion at sites AAW, LUC, and TOT generated by event 1222 (figure 8a), event 1005 (figure 8b) and event 0839 (figure 8c).

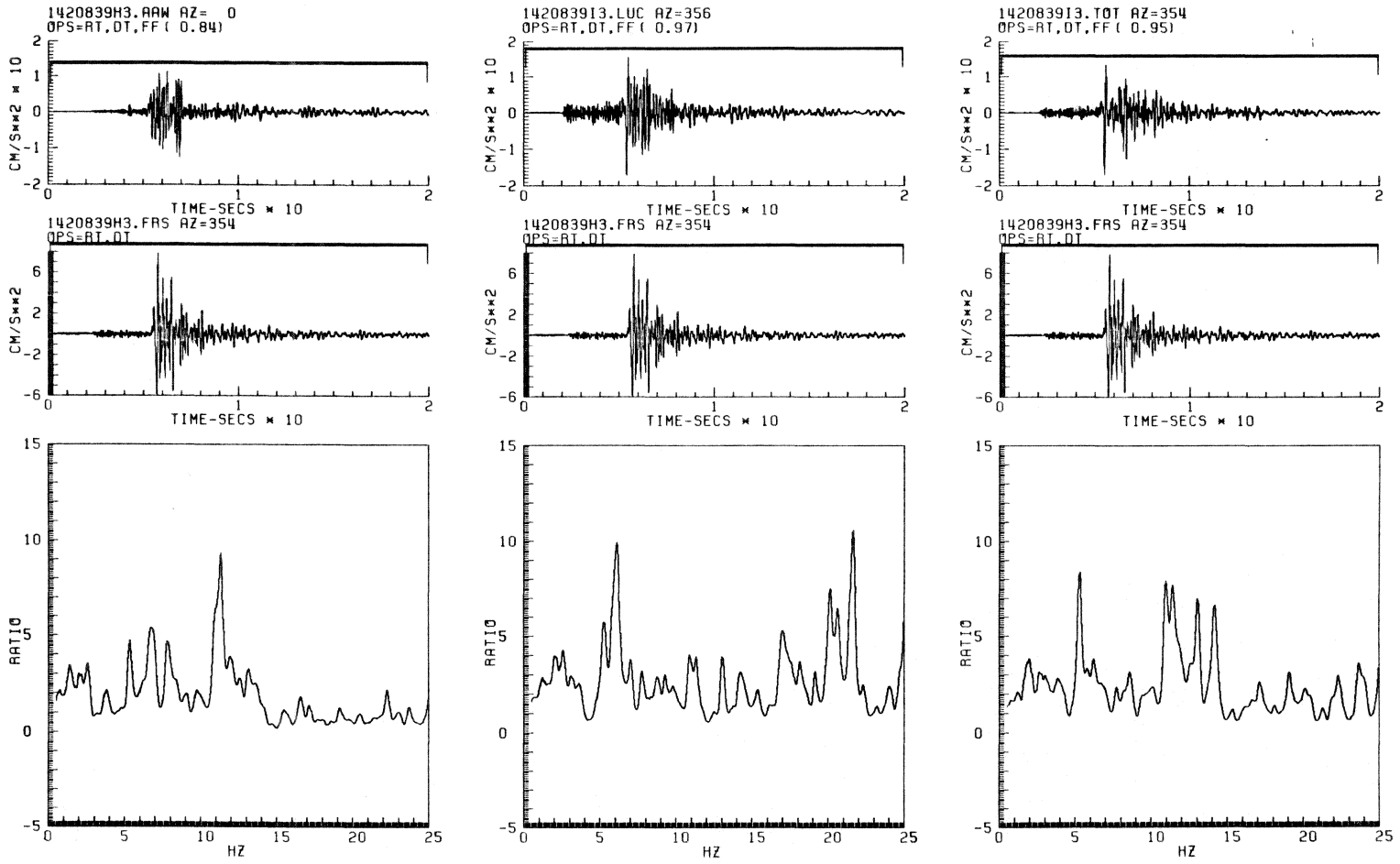

Figure 8c. Time histories and amplitude spectral ratios computed for transverse component of motion at sites AAW, LUC, and TOT generated by event 1222 (figure 8a), event 1005 (figure 8b) and event 0839 (figure 8c).

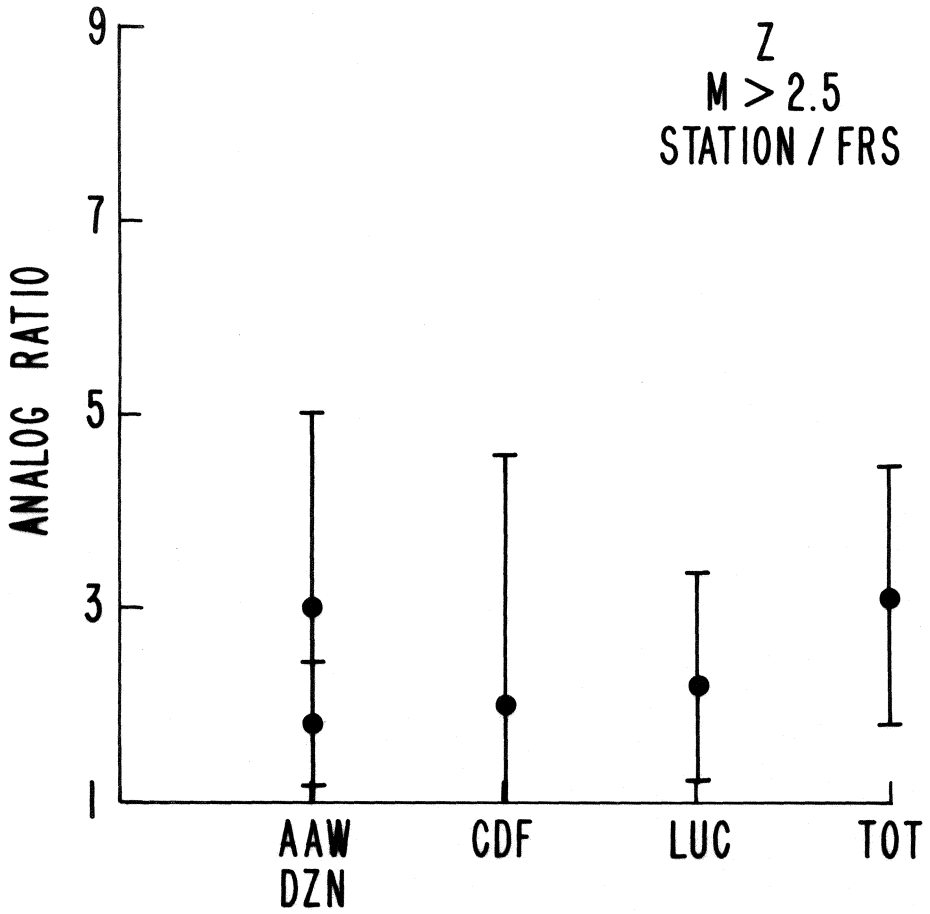

Figure 9a. Mean and standard deviation computed for analog ratios determined from recordings of the vertical component of ground motion for events of magnitude greater than 2.5 (table 2). The analog ratios are computed with respect to station FRS with corresponding corrections for geometrical attenuation.

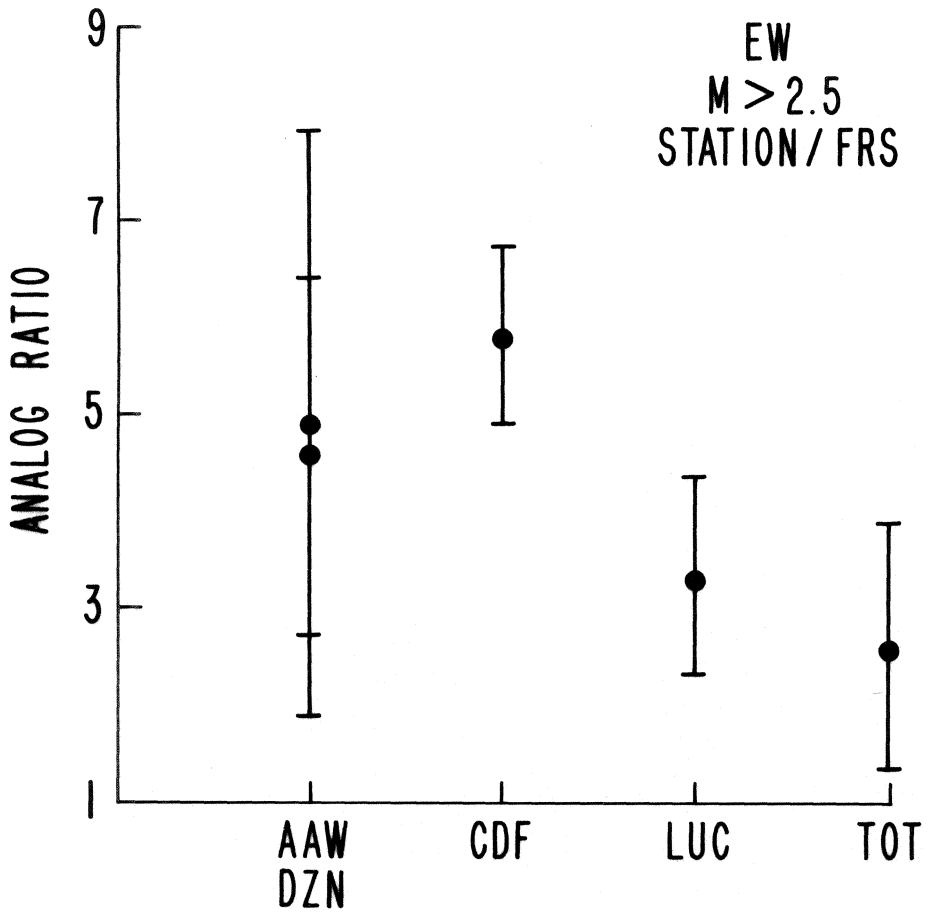

Figure 9b. Mean and standard deviation computed for analog ratios determined from recordings of the east-west horizontal component of ground motion for events of magnitude greater than 2.5 (table 2). The analog ratios are computed with respect to station FRS with corresponding corrections for geometrical attenuation.

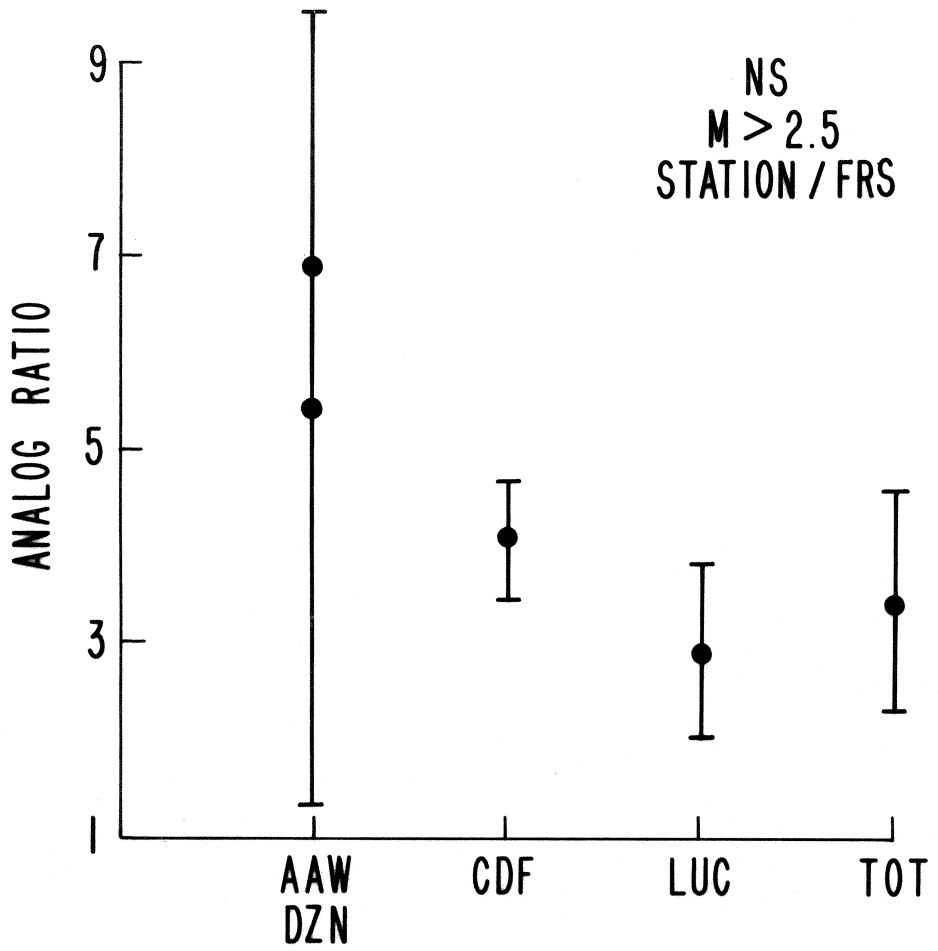

Figure 9c. Mean and standard deviation computed for analog ratios determined from recordings of the north-south horizontal component of ground motion for events of magnitude greater than 2.5 (table 2). The analog ratios are computed with respect to station FRS with corresponding corrections for geometrical attenuation.

Uncertainty in the estimates as measured by the computed standard deviations are in general largest for the sites in Coalinga. The small sample size (three events) for site CDF yields a relatively poor estimate of variability. Increased variability in the peak motions at the sites in Coalinga is consistent with strongly frequency-dependent amplification effects of the local soil deposits and azimuthal variations in basin response and propagation path as apparent from the computed spectral ratios (figures 6, 7, and 8). Even though the variability in the ratios of peak motions is considerable, their means suggest that the amplitudes of horizontal ground motions observed on alluvium in the community of Coalinga were significantly larger than those observed at the sandstone site FRS about 1 km from the margin of the alluvial basin. If similar amplification effects occurred during the May 2 event, then analog amplifications observed from the aftershocks suggest that the local site conditions beneath Coalinga could have been a contributory factor in the amounts of resultant damage.

The spectral ratios computed for three events (figures 6, 7, and 8) suggest that the calculated ground-motion spectra are strongly site and propagation path dependent with large frequency-dependent amplitude variations occurring over relatively short distances (< 1.5 km). Considerable amplification of the higher-frequency part of the spectrum (> 5 Hz) is apparent for the three components of motion at each of the sites.

The spectral ratios for the sites in Coalinga suggest average amplifications over the frequency band, 0.5-25 Hz, of about 2 (vertical), 4 (radial), and 3 (transverse) with larger average amplifications for the frequency band 1-15 Hz. The spectral ratios at these sites for the horizontal components of motion suggest the existence of several resonant frequencies with spectral amplifications greater than 10 in the frequency band 1-15 Hz. If these spectral ratios are indicative of the soil response at this site during the main event of May 2, then the suggested amplification at the higher frequencies 5-15 Hz may have been a contributing factor in the resulting damage to the older unreinforced masonry structures. Natural periods for the one and two story damaged structures are estimated to be in the range 0.05-0.2 sec (Scholl, oral commun.) based on previous studies by Scholl and Farhoomand (1972) and Blume, Sharpe, and Elasser (1961). The estimates of soil response at the Coalinga site presented here are preliminary and further study is

required to determine the extent to which they can be extrapolated to the main event.

ACKNOWLEDGEMENTS

The acquisition and analysis of this data set has been made possible by the dedicated efforts of a number of individuals. To mention only a few, Gary Maxwell and Grey Jensen have made outstanding contributions to the development of the GEOS system and Edward Cranswick has developed analysis procedures without which the timely analysis of this data set would not have been feasible. Gene Sembera provided field deployment and data recording expertise.

Table 2. Maximum and normalized peak-to-peak amplitudes recorded on Coalinga array ($M \geq 2.5$).

Event ID	Station ID	Maximum cm/s Z	Maximum cm/s NS	Maximum cm/s EW	Normalized (FRS) Z	Normalized (FRS) NS	Normalized (FRS) EW
140 0741 M = 3.0							
	LUC	.013	.022	.024	1.5	2.8	2.0
	TOT	.015	.017	.015	1.8	2.3	1.3
	FRS	.0077	.007	.011	1.0	1.0	1.0
140 1101 M = 3.2							
	AAW	.041	.077	.095	1.5	3.4	4.2
	LUC	.042	.042	.057	1.7	2.1	2.9
	TOT	.070	.057	.044	3.1	3.1	2.3
	FRS	.022	.018	.018	1.0	1.0	1.0
140 1222 M = 3.0							
	AAW	.032	.14	.15	1.6	9.6	4.4
	LUC	.034	.061	.090	1.9	4.6	2.9
	TOT	.042	.042	.048	2.5	3.3	1.6
	FRS	.016	.012	.028	1.0	1.0	1.0
141 1005 M = 3.2							
	AAW	.060	.29	.31	1.6	13.2	5.2
	DZN	.062	.27	.28	1.6	12.5	4.7
	LUC	.052	.097	.17	1.5	4.9	3.2
	TOT	.081	.092	.10	2.4	4.8	1.9
	FRS	.032	.018	.049	1.0	1.0	1.0
141 1629 M = 2.6							
	AAW	.026	.078	.073	3.4	14.0	11.5
	TOT	.016	.026	.013	2.5	5.5	2.4
	FRS	.0060	.0044	.0050	1.0	1.0	1.0
141 2000 M = 3.0							
	AAW	.058	.11	.13	1.9	3.1	3.6
	DZN	.050	.13	.11	1.7	3.7	3.2
	CDF	.054	.15	.17	1.9	4.5	5.1
	LUC	.063	.086	.13	2.4	2.8	4.2
	TOT	.056	.073	.070	2.2	2.5	2.4
	FRS	.023	.027	.027	1.0	1.0	1.0

Table 2. (Continued)

Event ID	Station ID	Maximum Z	Maximum NS cm/s	Maximum EW	Normalized (FRS) Z	Normalized (FRS) NS	Normalized (FRS) EW
142 0839 M = 4.3							
	AAW	.30	.70	.98	1.6	1.4	3.0
	DZN	.33	.75	.82	1.8	1.5	2.6
	LUC	.32	.94	.78	1.9	2.1	2.7
	TOT	.44	.96	.52	2.7	2.2	1.8
	FRS	.16	.41	.27	1.0	1.0	1.0
142 2103 M = 2.8							
	DZN	.050	.049	.076	6.3	5.4	7.5
	CDF	.039	.032	.063	5.2	3.7	6.4
	LUC	.035	.026	.047	4.7	3.1	4.9
	TOT	.044	.028	.055	6.1	3.4	5.9
	FRS	.0070	.0080	.0090	1.0	1.0	1.0
143 0925 M = 3.1							
	AAW	.013	.023	.013	1.3	3.8	2.4
	TOT	.036	.016	.015	4.3	3.1	3.2
	FRS	.0080	.0050	.0045	1.0	1.0	1.0
Average							
	AAW				1.8±0.7	6.9±5.2	4.9±3.0
	DZN				2.9±2.3	5.8±4.8	4.5±2.2
	CDF				3.6±2.3	4.1±0.6	5.8±0.9
	LUC				2.2±1.1	3.2±1.1	3.3±1.0
	TOT				3.1±1.3	3.4±1.1	2.5±1.4

REFERENCES

Blume, J. A., R. L. Sharpe, E. Elsasser (1961). A structural dynamic investigation of fifteen school buildings subjected to simulated earthquake motions, Division of Architecture, California.

Borcherdt, R. D. (1970). Effects of local geology on ground motion near San Francisco Bay: Bulletin of the Seismological Society of America, vol. 60, no. 1, pp. 29-61, February 1970.

Borcherdt, R. D., E. Cranswick (1983). Digital strong motion data recorded by U.S. Geological Survey near Coalinga in U.S. Geological Survey Open-File Report 83-511.

Borcherdt, R. D., J. B. Fletcher, C. W. Eckels, R. C. Brodine, J. R. Van Schaack, and R. E. Warrick (1979). A General Earthquake Observation System (GEOS-I), EOS, American Geophysical Union Transactions, v. 60, p. 889.

Eaton, J. P. (1983). Seismic setting, location and focal mechanism of the May 2, 1983, Coalinga earthquake in U.S. Geological Survey Open-File Report 83-511.

Scholl, R. E., and I. Farhoomand (1972). Observed dynamic response characteristics of residential structures: Project Trinidad, Report JAB-99-89, John a. Blume Associates, Engineers, San Francisco, California.